ELSEVIER

Contents lists available at ScienceDirect

International Journal of Non-Linear Mechanics

journal homepage: www.elsevier.com/locate/nlm



Self-induced parametric amplification in ring resonating gyroscopes

Pavel M. Polunin^{a,b,*}, Steven W. Shaw^{c,a,b}

- ^a Department of Mechanical Engineering, Michigan State University, East Lansing, MI 48823, USA
- b Department of Physics and Astronomy, Michigan State University, East Lansing, MI 48823, USA
- ^c Department of Mechanical and Aerospace Engineering, Florida Institute of Technology, Melbourne, FL 32901, USA

ARTICLE INFO

Keywords: Non-linear ring vibrations Disk resonator gyroscopes Parametric amplification Dispersive modal coupling

ABSTRACT

We investigate self-induced parametric amplification that arises from dispersive nonlinear coupling between degenerate modes in systems with circular symmetry that rotate about the axis of symmetry. This phenomenon was first observed in micro-electromechanical ring/disk gyroscopes, where it provided enhanced readout gain using purely passive nonlinear effects [Nitzan et al. [22], 2015]. The goal of this investigation is to provide a fundamental description of this phenomenon, which is an example where nonlinear dynamics can improve the performance of a practical device. To describe this behavior, we consider the in-plane vibrations of a thin ring surrounded by electrodes that rotates about its symmetry axis at a rate Ω much smaller than its vibration frequencies ω_m as is the case in applications. The focus is on the pair of degenerate elliptical modes, one of which is taken as the drive mode and the other as the sense mode for the sensor. These modes are coupled through both inertial (Coriolis) and geometric nonlinear effects, as described by general forms of the kinetic and potential energies that account for finite deformation kinematics, as well as electrostatic effects. We investigate the specific effects of this coupling on the system performance and its sensitivity when used as a sensor for the spin rate. Specifically, we show that drive mode vibrations with sufficiently high amplitude affect the sense mode dynamic behavior in the form of parametric pumping, which leads to a considerable amplification of the sense mode response. As this response amplitude is proportional to Ω , it results in a substantial increase of the gyroscope sensitivity with respect to the external angular rate. We also illustrate that the effects of the sense mode vibrations on the drive mode dynamics can be neglected in the model when $\Omega/\omega_n\ll 1$. Finally, we illustrate the applicability of our results by considering the dynamic response of a representative MEMS gyroscope model and quantifying the predicted benefits of these nonlinear effects.

1. Introduction

Studies of the linear and nonlinear vibrations of systems with circular symmetry have a long history and include papers on the transverse vibrations of plates, shells, membranes, rods, and tubes as well as the in-plane vibrations of plates and rings; see [1–4] and the research cited therein for a sampling of these works. This class of systems has applications in a number of areas such as antennae, pipes, and, most relevant to the present work, wine glass vibratory gyroscopes that use Coriolis effects to measure spin rates [5,6].

In recent decades there has been a desire to develop smaller versions of these gyroscopes, spurred by technological advancements in fabrication techniques and by increasing demands in commercial and military applications, which have led to a number of important advances in this technology space [7]. Prominent among these are developments in micro-electro-mechanical-system (MEMS) vibratory gyroscopes, which have shown great potential due to their small dimensions, favorable

power consumption, and high quality factors [8,9]. Generally, such devices are based on a micro-mechanical resonator with at least two matched resonant modes that interact via Coriolis effects [6]. Specifically, the resonator is forced to oscillate in one of its vibrational modes, called the drive mode, while the external rotation at Ω gives rise to Coriolis coupling between this mode and its symmetric partner, the sense mode, which is not driven by an external input. The vibrations of the sense mode thus have an amplitude proportional to Ω (when it is small as compared to the gyroscope operation frequency), and by measuring the amplitude of the readout signal from the sense mode, one can estimate Ω .

Improving the precision and accuracy of MEMS vibratory gyroscopes is a challenging task involving the precise matching of high-Q modal frequencies [10–12], compensation of quadrature errors that arise from coupling of the drive and sense modes [13–15], and optimizing the geometry of the resonator in order to achieve higher Q factors [16,17], to name a few. Also, all such devices are operated in the

^{*} Corresponding author at: Department of Mechanical Engineering, Michigan State University, East Lansing, MI 48823, USA. E-mail address: poluninp@msu.edu (P.M. Polunin).

linear operating regime, so as to avoid frequency shifts associated with nonlinearity. In this light, flexural-mode ring [13,18] and disk [19–21] vibratory gyroscopes offer significant advantages due to the inherent symmetry in their geometries and, consequently, symmetry of their drive and sense modes. Recent work on disk resonating gyroscopes (DRGs) has experimentally demonstrated that the gyroscope sensitivity to the external angular rate can increase significantly when the gyroscope is driven into a nonlinear operating regime [22]. The authors hypothesized that the observed phenomenon is due to parametric amplification [23–25] arising from nonlinear elastic coupling between the drive and sense modes of the device, which have nearly equal frequencies. In classical nonlinear vibrations, this is an example of autoparametric resonance [26–28].

The sensitivity S of a rate gyroscope, that is, the ratio of the amplitude of the sense signal to the angular rate Ω , is one the most important characteristics of sensor performance, since it, and the noise levels of the device, quantify the resolution of the sensor in terms of the lower end of the angular velocities that can be detected [6]. Thus, there is strong motivation to understand, from a fundamental point of view, the advantageous effects of the self-induced amplification of the sense signal observed in [22], especially since it appears to be the fortuitous result of passive nonlinear behavior, requiring no additional sensing or actuation. This is precisely the goal of the investigation described in this paper.

Nonlinear modal coupling is a well-known phenomenon in the theory of nonlinear vibrations and it has been thoroughly studied in a wide variety of systems [29], including micromechanical systems [30-33]. It generally occurs in resonators experiencing vibration amplitudes at which nonlinear strain-displacement relationships, or other nonlinear effects, couple two or more vibrational modes. Furthermore, specific research on the nonlinear vibrations of spinning ring-like geometries has illustrated the rich dynamics associated with the inplane flexural modes of these structures [34-37]. In this paper we analyze the dynamic behavior of the elliptical modes in ring/disk resonating gyroscopes to explain and explore self-induced parametric amplification in these systems [22]. In particular, we use a model of the resonator consisting of a thin ring spinning about its axis of radial symmetry with electrostatic forces arising from capacitive actuation/ sensing schemes. Using finite deformation kinematics, we show that the elliptical drive and sense modes are nonlinearly coupled through both stiffness (including electrostatic contributions) and inertial terms. Next, we show that the general case of mode-coupled dynamics can be simplified by neglecting the back-action of the sense mode motion on the drive mode (due to their differing amplitudes), and provide conditions for which this approximation holds. In this simplified picture, we discuss the effect of inertial nonlinearities on the drive mode dynamics and show how nonlinear modal interactions lead to parametric amplification of the sense mode, and thus to an increase in the gyroscope sensitivity.

The remainder of the paper is organized as follows. In Section 2, we formulate a model for resonator geometries that support a pair of degenerate (equal frequency) n=2 radial modes. In Section 3 we consider the nonlinear in-plane flexural vibrations of a thin spinning ring in the presence of electrostatic actuation. A detailed analysis of the dynamic behavior of the drive and sense modes is given in Sections 3.2 and 3.3, respectively. Finally, in Section 3.4 we illustrate the applicability of our results to a model of the representative ring resonating gyroscope reported in [18], and concluding remarks are given in Section 4.

2. Model

In this section we present an analytical framework which can be used to derive equations of motion for the in-plane vibration modes of interest for ring/disk resonating gyroscopes. Such a formulation is advantageous since it can be applied to systems with relatively simple

geometries, such as a thin ring or a solid circular plate, as well as to MEMS gyroscopes with less trivial geometries; see, for example, [38]. We start our analysis by introducing a cylindrical coordinate system (r, θ, z) and consider a gyroscope with generic geometry that supports a pair of degenerate elliptical modes each of which has two nodal diameters, which we denote with modal coordinates A and B and mode shapes described by $\Xi_A(r, \theta) = \xi(r)\cos 2\theta$ and $\Xi_B(r, \theta) = \xi(r)\sin 2\theta$ so that their nodal diameters are separated by $\pi/4$ [22]. Without loss of generality, we designate these as the drive (A) and sense (B) modes, respectively.

During gyroscope operation, the shape of the resonator vibration changes as it experiences displacements in the radial, $u=u(r,\theta,t)$, and circumferential, $v=v(r,\theta,t)$, directions, which we assume to be independent of the out-of-plane coordinate z. These displacements can be expressed in terms of the modal coordinates A(t) and B(t) in a manner that depends on the gyroscope geometry, as $u=u(r,\theta,A(t),B(t))$ and $v=v(r,\theta,A(t),B(t))$. Generally, both u and v can be nonlinear in v and v can be be obtained with certain assumptions for relatively simple structures like a thin ring, see Section 3, or a solid circular plate [2,39,40], while in the case of non-trivial geometries, computing similar expressions generally requires the use of finite element methods.

In this paper we utilize Lagrange's method to derive the equations that govern the drive and sense modes of the gyroscope using generalized coordinates $q_{1,2}=A,\,B$ to express the nonlinear equations of motion for the gyroscopic elliptical modes. The kinetic energy of the system is computed using standard methods [41,39] and is given by

$$T = \frac{1}{2} \iiint_{V} \rho[(\dot{u} - v\Omega)^{2} + (\dot{v} + (r + u)\Omega)^{2}] r dr d\theta dz, \tag{1}$$

where Ω is the external angular rate about the z- axis, $\rho=\rho(r,\theta)$ is the resonator material mass density, which is assumed to be uniform in z, and V is the volume of the resonator body. The potential energy of the gyroscope consists of elastic U_d and electrostatic U_e components. The electrostatic part results from electrostatic interaction of the resonator body with the drive/sense electrodes. Generally, the electrode gap size Δ is much smaller that the outer radius of the resonator R_o and the z thickness of the resonator, so that one can neglect the curvature of the electrodes and apply a local parallel-plate approximation. We also assume that Δ is uniform along the gyroscope circumference. In this case, the electrostatic potential energy becomes

$$U_{e} = -\frac{\epsilon_{0}}{2} \int_{0}^{2\pi} d\theta b(R_{o}, \theta) R_{o} \frac{(V_{DC} + V_{AC}(\theta))^{2}}{\Delta - u(R_{o}, \theta)}, \qquad (2)$$

where $b(R_o, \theta)$ is the z thickness profile of the gyroscope body along its circumference, V_{DC} and V_{AC} represent magnitudes of the bias and periodic voltages used for the electrostatic actuation and sensing and $\epsilon_0 = 8.85 \times 10^{-12} \, \text{F/m}$ is the vacuum permittivity.

Mechanical deformations of the resonator body and the associated stresses contribute to the elastic potential energy in the form of a deformation potential U_d . For in-plane vibrations, U_d can be found as, [39].

$$U_d = \frac{1}{2} \iiint_V (\sigma_{rr} \epsilon_{rr} + \sigma_{\theta\theta} \epsilon_{\theta\theta} + \sigma_{r\theta} \epsilon_{r\theta}) r dr d\theta dz, \tag{3}$$

where $\epsilon_{ij} = \epsilon_{ij}(u, v)$ and $\sigma_{ij} = \sigma_{ij}(u, v)$ are the strain and stress in the body. Hooke's law establishes the well-known relationships between these quantities,

$$\begin{split} & \sigma_{rr} = E^*(\varepsilon_{rr} + \nu \varepsilon_{\theta\theta}), \\ & \sigma_{\theta\theta} = E^*(\varepsilon_{\theta\theta} + \nu \varepsilon_{rr}), \\ & \sigma_{r\theta} = G\varepsilon_{r\theta}, \end{split} \tag{4}$$

where $E^* = E(1-\nu^2)^{-1}$ and G are the effective normal and shear moduli, respectively. In order to analyze the nonlinear dynamic behavior of the gyroscopic radial modes, one necessarily has to account for higher-

order terms in the strain tensor $\epsilon_{ij}(u,\nu)$. Using finite deformation theory (see Appendix A) one can show that the nonlinear strain-displacement relationships, up to the second order in u and v, are given by

$$\epsilon_{rr} = \frac{\partial u}{\partial r} + \frac{1}{2}r^2 \left(\frac{\partial}{\partial r} \frac{v}{r}\right)^2,$$
 (5a)

$$\epsilon_{\theta\theta} = \frac{u}{r} + \frac{\partial v}{r\partial\theta} + \frac{1}{2} \left(\frac{\partial u}{r\partial\theta}\right)^2 + \frac{u}{r} \frac{\partial v}{r\partial\theta},$$
(5b)

$$\epsilon_{r\theta} = \frac{\partial v}{\partial r} + \frac{\partial u}{r\partial \theta} - \frac{v}{r} - \frac{uv}{r^2} - \frac{u}{r} \frac{\partial u}{r\partial \theta} - \frac{\partial u}{r\partial \theta} \frac{\partial v}{r\partial \theta} + \frac{v}{r} \frac{\partial u}{\partial r} + \frac{u}{r} \frac{\partial v}{\partial r} - \frac{\partial u}{\partial r} \frac{\partial v}{\partial r}.$$
(5c)

Since the resonator displacements u and v are functions of the modal coordinates A and B, the Lagrangian for the system becomes, after integration over the resonator volume, $L = L(A, B, \dot{A}, \dot{B})$. By substituting this form of L into Lagrange's equations, one can immediately obtain equations of motion for the gyroscopic elliptic modes. In Section 3 we apply this procedure to a simple model of a thin inextensible ring, which, as we show, is sufficient to demonstrate the self-induced amplification phenomenon, and is amenable to detailed analysis. However, as noted above, this analytical approach is sufficiently general to be used for analyzing gyroscopes with different resonator shapes, such as rings with supporting spring elements [18], circular plates of non-uniform thickness in the z- direction, and other complex geometries [22,38].

3. Forced nonlinear vibrations of elliptical modes of a thin spinning ring

3.1. Gyroscope dynamics with fully-coupled modes

We apply the general formulation of Section 2 for analysis of the nonlinear in-plane vibrations of the elliptical modes of a uniform (ρ, b, h) , and Δ are constants) circular ring rotating at a constant speed Ω about the z- axis in the presence of electrostatic forces from electrodes, as depicted in Fig. 1. Hereafter, we employ a thin ring approximation, i.e., $h \ll R$, where h and R are the ring radial thickness and its mid-line radius, respectively. In this case we can apply results for the vibrations of shallow shells [39], and neglect the stress in the radial direction, $\sigma_{rr}=0$, as well as the shear stress, $\sigma_{r\theta}=0$. The application of these

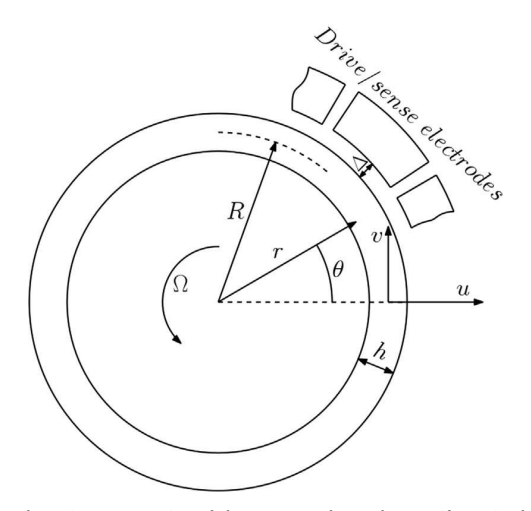


Fig. 1. Schematic representation of the system under study: a uniform circular ring rotating at a constant angular rate Ω about the z- axis with segmented electrodes representing the means for electrostatic actuation and readout. Segmentation of electrodes is an essential feature of the device structure necessary for producing modal driving force through $V_{AC}(\theta, t)$ and tuning the gyroscopic drive and sense modes via a non-uniform distribution of the bias voltage $V_{DC}(\theta)$ [22].

assumptions in Eq. (4) yields $\sigma_{\theta\theta}=E\varepsilon_{\theta\theta}$, which is the same expression as that for the longitudinal stress/strain relationship for the transverse bending of an Euler-Bernoulli beam. Following the bending theory for thin shells, we express the radial and circumferential displacements of any point of the ring as

$$u(r, \theta, t) = u(\theta, t),$$

$$\nu(r, \theta, t) = \nu_0(\theta, t) + \delta\nu_1(\theta, t),$$
(6)

where $\delta=r-R$ is the radial coordinate relative to the ring mid-line, ν_0 is the circumferential displacement of a point on the ring mid-line, and ν_1 is the slope of the tangential displacement profile across h. Similar to ν , we approximate the strain field in the θ direction as a linear function of δ , i.e., $\epsilon_{\theta\theta}=\epsilon_{\theta\theta}^{(0)}+\delta\epsilon_{\theta\theta}^{(1)}$, where $\epsilon_{\theta\theta}^{(0)}$ represents the midline stretching of the ring, while $\epsilon_{\theta\theta}^{(1)}$ represents the strain due to the ring bending. It is known that the ring mid-line stretching has a negligible effect on the ring dynamics, so long as the wavelength of the vibration mode is large as compared with its thickness h [34,39,42]. Since we are interested in the dynamic behavior of elliptical (n=2) gyroscopic modes, this condition is satisfied for a thin ring. Therefore, to simplify the analysis, we make the reasonable assumption that the ring is inextensible on its mid-line, so that $\epsilon_{\theta\theta}^{(0)}=0$.

Applying these assumptions, we can write the elastic potential energy of the resonator body as,

$$U_{d} = \frac{EI}{2R^{3}} \int_{0}^{2\pi} d\theta \left[u + \frac{\partial^{2} u}{\partial \theta^{2}} - \frac{1}{2R} \left(\frac{\partial u}{\partial \theta} \right)^{2} \right]^{2}, \tag{7}$$

where $I = bh^3/12$ is the second moment of area of the ring cross-section [41]

Considering U_e for this geometry, we assume that radial ring deflections are small compared to the gap size, $u\ll \Delta$, which is frequently the case for capacitively-driven MEMS resonators. From this we obtain the approximate expression for the electrostatic contribution to the system potential energy

$$U_e \approx -\frac{\epsilon_0 bR}{2\Delta} \sum_{n=0}^4 \int_0^{2\pi} d\theta (V_{DC} + V_{AC}(\theta, t))^2 \frac{u^n(\theta, t)}{\Delta^n}, \tag{8}$$

where we have expanded the denominator up to the fourth order in u in order to account for the same order nonlinear terms as in U_d . Note that in practice the electrodes are only on the outside of the ring, which results in a slight expansion of the ring in its radial direction. However, typical circumferential strains due to the presence of the V_{DC}^2 term in Eq. (8) are rather small; in fact, $\epsilon_{\theta\theta}^{(0)} \sim 10^{-8}$ for the representative system considered in Section 3.4, which corresponds to the change of the ring radius by 0.06 nm. Given that fabrication tolerances for modern MEMS resonators are $\gtrsim 10$ nm, such small deformation of the ring due to the bias voltage can be neglected, which justifies our assumption that the ring is inextensible.

In the case of the thin ring, the mode shapes for the elliptical modes become independent of r and are given by $\Phi_A(\theta) = \cos 2\theta$ and $\Phi_B(\theta) = \sin 2\theta$, Fig. 2. Using these mode shapes, we can express the

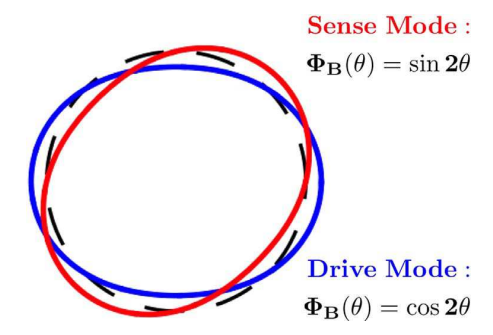


Fig. 2. Degenerate elliptical modes of the uniform circular ring under study.

radial deflection of the ring body as

$$u(\theta, t) = A(t)\cos 2\theta + B(t)\sin 2\theta + C(t), \tag{9}$$

where the time-dependent function C(t) is included in order to ensure periodicity of $v(\theta,t)$ in θ [34,36]. Note that the expression for C(t) is obtained by solving $\epsilon_{\theta\theta}^{(0)}=0$, see Eq. (5b), and has the form $C(t)\approx -(A^2(t)+B^2(t))/R$. Using this form for the radial displacement, and assuming that the oscillating actuation voltage across the electrodes has a spatial dependence matching the drive mode, that is, $V_{AC}(\theta,t)=V_{AC}(t)\cos 2\theta$, with $|V_{AC}(t)|\ll V_{DC}^{-1}$ and $\Delta\ll R$, we use Lagrange's method with the kinetic energy in Eq. (1) and potential energy $U=U_e+U_d$ to obtain nonlinear equations of motion governing the n=2 elliptical modes of the ring. After dividing through by the

modal mass
$$m_{A,B} = \left(\frac{5}{4}\right)\pi\rho bhR$$
, these take the form
$$\ddot{A}\left[1 + \frac{3}{5R^2}(11A^2 + B^2)\right] + \dot{A}\left[2\Gamma_A + \frac{6B\dot{B}}{5R^2}\right] + A\omega_0^2$$

$$+A\left[\Omega^2\left(\frac{11}{5} - \frac{37B^2}{10R^2}\right) + \kappa\frac{B^2}{R^2} + \frac{33\dot{A}^2}{5R^2} + \frac{31\dot{B}^2}{5R^2} + \frac{34B\ddot{B}}{5R^2}\right]$$

$$+\frac{A^3}{R^2}[y - \frac{33}{10}\Omega^2] - \frac{16\dot{B}}{5R^2}\Omega A^2$$

$$= \frac{8}{5}\Omega \dot{B}\left(1 - 2\frac{B^2}{R^2}\right) + F_A(A, B, t),$$

$$\ddot{B}\left[1 + \frac{3}{5R^2}(11B^2 + A^2)\right] + \dot{B}\left[2\Gamma_B + \frac{6A\dot{A}}{5R^2}\right] + B\omega_0^2$$

$$+B\left[\Omega^2\left(\frac{11}{5} - \frac{37A^2}{10R^2}\right) + \kappa\frac{A^2}{R^2} + \frac{33\dot{B}^2}{5R^2} + \frac{31\dot{A}^2}{5R^2} + \frac{34A\dot{A}}{5R^2}\right]$$

$$+\frac{B^3}{R^2}[y - \frac{33}{10}\Omega^2] - \frac{16\dot{A}}{5R^2}\Omega B^2$$

where

 $= -\frac{8}{5} \Omega \dot{A} \left(1 - 2 \frac{A^2}{R^2} \right) + F_B(A, B, t),$

$$\begin{split} \omega_{0}^{2} &= \frac{1}{5\rho} \left(3\frac{Eh^{2}}{R^{4}} - 4\frac{\epsilon_{0}V_{DC}^{2}}{h\Delta^{3}} \right), \\ \gamma &= \kappa = \frac{6R^{2}}{5\rho} \left(\frac{Eh^{2}}{R^{6}} - \frac{\epsilon_{0}V_{DC}^{2}}{h\Delta^{5}} \right), F_{A}(A, B, t) = \frac{\epsilon_{0}V_{AC}(t)V_{DC}}{5\rho h\Delta^{2}} \left(4 + \frac{3B^{2}}{\Delta^{2}} + \frac{9A^{2}}{\Delta^{2}} \right) \\ , F_{B}(A, B, t) &= \frac{\epsilon_{0}V_{AC}(t)V_{DC}}{5\rho h\Delta^{4}} AB. \end{split}$$
(11)

Here ω_0 is the natural frequency of the modes, γ is the effective modal Duffing coefficient, and κ is the strength of the intermodal dispersive coupling, all of which account for both elastic and electrostatic stiffnesses and are normalized by the modal mass.2 The linear and nonlinear stiffness coefficients represent combined effects from the elastic deformation and electrostatic effects. Terms F_A and F_B represent the periodic excitation acting on the drive and sense modes, respectively. Note that the drive mode has both direct and (nonlinear) parametric components, while the sense mode is driven in a purely nonlinear parametric manner, since the excitation is taken to be perfectly aligned with the (linear) drive mode. These nonlinear terms in the modal forces $F_{A,B}$ result from the nonlinear treatment of the electrostatic potential energy. In order to complete the model, we have introduced phenomenological linear dissipation coefficients Γ_A and Γ_B for the modes. The analysis of Eqs. (10a) and (10b) in their full form is quite challenging, due to the fact that the equations are nonlinear and coupled through multiple terms, including elastic, inertial, and even the external driving terms; see Eq. (11).

In order to obtain further insight into the gyroscope dynamics and obtain a better understanding of the self-induced amplification phe-

nomenon, we use the fact that the drive mode is directly driven to an amplitude that is much larger than the amplitude that will be experienced by the sense mode. In fact, the sense mode is driven by the vibrations of the drive mode through the Coriolis term proportional to $\Omega\dot{A}$ (the first term on the right hand side of Eq. (10b)), and also parametrically through coupling terms like $\kappa BA^2/R^2$. In this case the relative phase between these two terms is $\pi/4$, which indicates, following the analysis in [23], that the sense mode response will be amplified by the drive mode vibrations regardless of their amplitude. When the parametric drive is weak enough, meaning that A is sufficiently small, the response of the sense mode due to the Coriolis effect remains stable and these parametric terms amplify the sense mode response [24,25,43]. Consequently, if the gyroscope is exposed to angular rates that satisfy $\Omega \ll \omega_0$ (typical values for the rate grade gyroscopes [7] are $\Omega \sim 1$ Hz and $\Omega/\omega_0 \lesssim 10^{-5}$), we can assume that the sense mode operates in its linear regime. Note that $\Omega \ll \omega_0$ also allows us to neglect terms proportional to Ω^2 in Eqs. (10a) and (10b). In contrast, the gyroscopic drive mode can operate at amplitudes where nonlinear effects come into play. In fact, this must be the case in order to achieve the desired amplification of the sense mode. Under these conditions, the back action of the sense mode on the drive mode can be neglected, and we can analyze the dynamics of the drive mode independently. In fact, numerical analysis of (10a) and (10b) shows that already for $\Omega/\omega_0 \sim 10^{-4}$ this assumption results in only $\lesssim 3\%$ error in the drive mode amplitude in the vicinity of its nonlinear resonance; see Fig. 3. As expected, when the back-action from the gyroscope sense mode is retained in the model, the drive mode frequency response exhibits a (minor) second peak in the vicinity of the sense mode vibration frequency due to two-way interaction between gyroscopic modes. However, since the drive mode operating point is near its nonlinear resonance, the effect of this back-coupling leads to rather small perturbation of the drive mode amplitude and no change in stability, thus, we can employ a model with one-way coupling when $\Omega \ll \omega_0$. After obtaining the (nonlinear) solution for the drive mode, we can analyze the response of the gyroscopic sense mode and study the self-induced amplification and associated increase of the gyroscope

3.2. Dynamics of the drive mode

Here we study the dynamic behavior of the drive mode of the ring and analyze the effects of inertial nonlinearities and nonlinear forcing terms on its behavior. Using the assumptions derived above, we neglect coupling to the sense mode in Eq. (10a) and assume relatively slow external rotation, $\Omega \ll \omega_0$, to obtain the following nonlinear model for the drive mode behavior

$$\ddot{A}\left(1 + \mu \frac{A^2}{R^2}\right) + 2\Gamma_A \dot{A} + A\left(\omega_A^2 + \mu \frac{\dot{A}^2}{R^2} + \gamma \frac{A^2}{R^2}\right)
= F\cos(\omega t + \phi_F) \left(1 + C_{FA} \frac{A^2}{A^2}\right),$$
(12)

where μ is the strength of the inertial nonlinearity and C_{FA} represents the nonlinear correction to the modal forcing. Additionally, the drive frequency is near the modal natural frequency, that is, $\omega = \omega_A + \delta \omega$ with $\delta \omega \ll \omega_A$. Note that in Eq. (12) we keep all coefficients in a generic form to keep the formulation general, but apply the results for the ring geometry below.

In order to analyze Eq. (12), we note that the system is lightly damped (typical damping ratios are in the range $10^{-5} - 10^{-4}$), resonantly driven, and has cubic stiffness and inertial nonlinearities, so the problem is treated in the standard way. We start by representing the modal displacement in the form $A(t) = a(t)R\cos(\omega t + \phi_A(t))$, where $(a(t), \phi_A(t))$ are the non-dimensional vibration amplitude and the phase of the drive mode response. By employing the method of averaging [44], we assume that $(a(t), \phi_A(t))$ change slowly over times $\sim \omega_A^{-1}$ and let

(10b)

¹ This assumption is convenient but not necessary, since a general distribution can be projected onto the modes of interest.

projected onto the modes of interest. 2 Coefficients κ and γ are, not by coincidence, equal, but we keep their designation distinct since they have different effects on the system response.

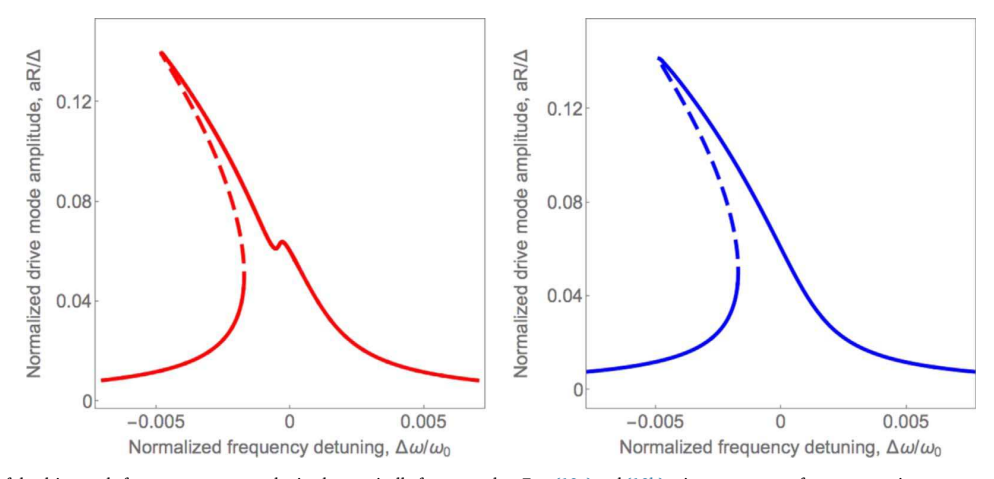


Fig. 3. Comparison of the drive mode frequency responses obtained numerically from complete Eqs. (10a) and (10b) using parameters of a representative gyroscope from Section 3.4 (left panel) and by neglecting back-action from the gyroscope sense mode (right panel). Note that the amplitude differences are small and, more importantly, neglecting the coupling does not affect the stability of the response.

 $\dot{A}(t) \approx -\omega a(t)R\sin(\omega t + \phi_A(t))$. By using these expressions for A(t) and $\dot{A}(t)$ in Eq. (12) and disregarding fast-oscillating terms, we obtain equations governing (a,ϕ_A) on the slow time scale $\sim \Gamma_A^{-1}$. The steady-state responses found from these equations can be solved to obtain the following expression that relates drive mode response amplitude to the system and input parameters,

$$\delta\omega(a) \approx \frac{\frac{3a^2}{8\omega_A} \left(\gamma - \frac{2}{3}\mu\omega_A^2\right)}{1 - \frac{1}{4}\mu a^2} \pm \frac{\left|\frac{4\Delta^2 + 3C_{FA}a^2R^2}{4\Delta^2 + 1C_{FA}a^2R^2}\right| \sqrt{\frac{F^2(4\Delta^2 + C_{FA}a^2R^2)^2}{8a^2R^2\Delta^4\omega_A^2} - \Gamma_A^2}}{1 - \frac{1}{4}\mu a^2}.$$
(13)

As expected, the nonlinear forcing term does not affect the shape of the modal backbone curve, represented by the first term in Eq. (13), but alters the shape of the frequency response branches and renormalizes the effective modal forcing amplitude. Simplification of Eq. (13) can be made when the modal amplitude is small compared with the electrode gap size, that is, when $a \ll \Delta/R$, as is common in applications (to avoid pull-in [45,46]). In this case, the nonlinear correction to the drive mode forcing can be safely neglected, $C_{FA} = 0$, an assumption we employ in the following development.

It is important to recognize that the amplitude-dependent shift of the free vibration frequency of the modes has the following sources: the stiffness Duffing nonlinearity $\gamma=\gamma_d+\gamma_e$, where γ_d and γ_e are the contributions from elastic and electrostatic stiffness effects, respectively (see Eq. (11)), and inertial nonlinearities which have an effective Duffing nonlinearity $\gamma_i=-\frac{2}{3}\mu\omega_A^2$ (see Eq. (13)). The inertial nonlinear effects have the same origin (finite deformation kinematics) as the nonlinearities in the elastic deformation potential, and we combine these effects into a single mechanical contribution to the modal Duffing constant, denoted $\gamma_m=\gamma_d+\gamma_i$. For moderate vibration amplitudes, the steady-state amplitude response is that of an equivalent Duffing system and can be expressed as

$$\omega(a) \approx \omega_A + \frac{3a^2}{8\omega_A} (\gamma_m + \gamma_e) \pm \sqrt{\left(\frac{F}{2aR\omega_A}\right)^2 - \Gamma_A^2},\tag{14}$$

examples of which are shown in Fig. 4.

Analysis shows that inertial nonlinearities must be taken into account when $|\gamma_e| \lesssim |\gamma_m|$, which can be the case in resonators with large mechanical stiffness, like circular plates. Interestingly, when the electrostatic potential provides only small corrections to both linear and nonlinear stiffness constants, inertial nonlinearities have a dominant effect on the modal frequency response and cause substantial

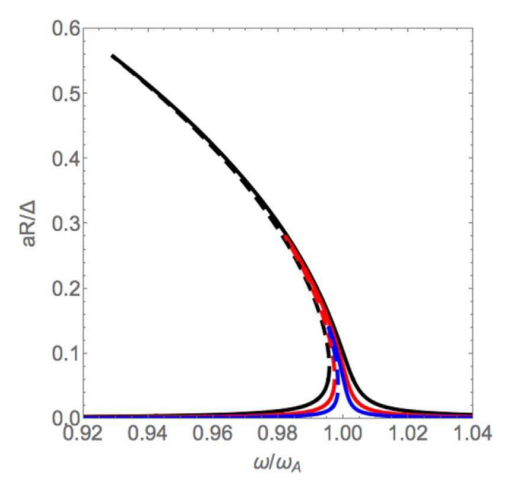


Fig. 4. Representative steady-state frequency response curves of the ring drive mode described by Eq. (14) for different values of the forcing amplitude F. The blue, red, and black curves correspond to forcing magnitudes F_0 , $2F_0$, $4F_0$. Responses are obtained under the assumption that electrostatic forces dominate the Duffing nonlinearity, i.e., $|\gamma_e| \gg |\gamma_m|$. Solid and dashed curves represent stable and unstable response amplitudes. (For interpretation of the references to color in this figure legend, the reader is referred to the web version of this article.)

softening of the resonator frequency. Specifically, for the ring $\gamma_d=2\omega_A^2$ and $\gamma_m=-\frac{12}{5}\omega_A^2$. Note that a similar situation occurs in cantilever type resonators where inertial nonlinearities essentially dominate the dynamic behavior of the fundamental mode and cause the vibration frequency to soften as a function of vibration amplitude [47,48]. On the other hand, when $|\gamma_e|\gg |\gamma_m|$, electrostatic effects dominate the nonlinear dynamics of the system, so that the nonlinear terms arising from mechanics, both inertial and elastic stiffness, can be neglected, in which case we use the approximation $\gamma_m\approx 0$, which we will use in Section 3.4.

3.3. Dynamics of the sense mode: parametric amplification

In this section we analyze the response of the gyroscopic sense mode B, using the drive response as an effective excitation. This excitation has components from Coriolis coupling from the external angular rate Ω ,

and from nonlinear dispersive coupling from elastic, inertial, and electrostatic effects. In what follows, we assume that the drive mode motion can be represented as, $A(t) = aR\cos(\omega t + \phi_A)$, where a and ϕ_A are the drive mode steady-state amplitude and phase, respectively. When Ω is small as compared with the gyroscope operation frequency, i.e., $\Omega \ll \omega$, and the parametric pumping does not destabilize the sense response, the dynamic behavior of the sense mode is governed by the following equation of motion, obtained from Eq. (10b),

$$\ddot{B} + \dot{B} \left(2I_B + C_I \frac{A\dot{A}}{R^2} \right) + B \left(\omega_B^2 + C_d \frac{A^2}{R^2} + C_1 \frac{\dot{A}^2}{R^2} + C_2 \frac{A\ddot{A}}{R^2} \right) = C_{\Omega} \Omega \dot{A}, \tag{15}$$

where we have employed linearized dynamics for B (justified in Section 3.1). This model has direct (Coriolis) excitation from \dot{A} and parametric excitation from nonlinear combinations of (A, \dot{A}, \ddot{A}) . The C_j are constants that depend on the geometry of the gyroscope body. Since Eq. (15) contains both direct and parametric resonant driving terms, it is convenient to represent the sense mode response in the form $B = R(b \exp[i\omega t] + c. c.)$ and apply method of averaging in the manner in [23]. After averaging and some manipulations we obtain the following expression for the steady-state amplitude of the sense mode

$$|b| = |C_{\Omega}|\Omega a \frac{\omega}{2} \frac{\sqrt{4\omega^2 \Gamma_B^2 + (\omega_n^2 - \omega^2 + \lambda)^2}}{|4\omega^2 \Gamma_B^2 + (\omega_n^2 - \omega^2)^2 - \lambda^2|},$$
(16)

where $\omega_n^2 = \omega_B^2 + \frac{1}{2}a^2(C_d + \omega^2(C_1 - C_2))$ is the effective vibration frequency of the sense mode, which is modified by nonlinear coupling to the drive mode at amplitude a, and $\lambda = \frac{1}{4}a^2(C_d + \omega^2(C_T - C_1 - C_2))$ is the strength of the parametric pumping due to the coupling to the drive mode. Note that both ω_n^2 and λ are determined by the system nonlinearities, the drive vibration amplitude a, and the gyroscope operation frequency ω . This expression describes the amplitude of the sense mode and captures the interaction of the effects of the direct (Coriolis) drive and the parametric pumping from nonlinear coupling.

Analysis of Eq. (16) reveals some important features. First, when the drive mode vibration amplitude is sufficiently small such that one can neglect the effect of the parametric pumping, that is, λ can be neglected, the expression for the sense mode amplitude becomes

$$|b|_{l} = \frac{a\omega |C_{\Omega}|\Omega}{2\sqrt{(\omega_{B}^{2} - \omega^{2})^{2} + 4\omega^{2}\Gamma_{B}^{2}}},$$
(17)

which represents the case when both modes behave like linear resonators. In this light, it is convenient to express the gyroscopic sense mode amplitude in the more general case as follows

$$|b|_{par} = G|b|_{l}, G = \frac{\sqrt{[4\omega^{2}\Gamma_{B}^{2} + (\omega_{n}^{2} - \omega^{2} + \lambda)^{2}][(\omega_{B}^{2} - \omega^{2})^{2} + 4\omega^{2}\Gamma_{B}^{2}]}}{|4\omega^{2}\Gamma_{B}^{2} + (\omega_{n}^{2} - \omega^{2})^{2} - \lambda^{2}|},$$
(18)

where G is the amplification of the sense mode, i.e., the gain, that arises from the parametric coupling to the drive mode. This gain from the coupling is illustrated in Fig. 5, which shows the sense mode response amplitude for the case where the coupling is ignored (black dashed lines) and for two levels of coupling (red and blue lines). Here the parametric amplification is evident, as is the frequency shift that arises from the coupling; see Eq. (15). A more complete representation of the gain is considered below.

Another feature associated with Eq. (16) is that the system gain G or, equivalently, the sense mode amplitude $|b|_{par}$ diverges when the denominator in Eq. (18) vanishes, i.e. $(4\omega^2\Gamma_B^2 + (\omega_n^2 - \omega^2)^2 - \lambda^2) \to 0$. By solving this equation, one obtains the parametric instability condition expressed in terms of the drive parameters as (a^*, ω^*) , corresponding to $G \to \infty$. This (a^*, ω^*) condition corresponds to the case where the parametric coupling terms in Eq. (15) result in instability of the sense mode [29]. As this instability is approached, the linearized version of the sense mode model, given by linearizing Eq. (15), is insufficient to describe the sense mode dynamics and the full coupled form of the

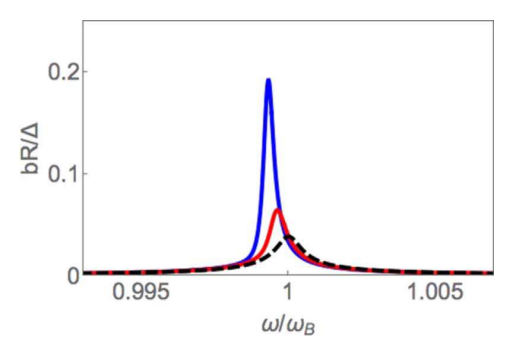


Fig. 5. Effect of self-induced parametric amplification on frequency responses of the ring sense mode described by Eq. (16) for different values of the dispersive modal coupling coefficient C_d , where we consider the case $C_d/\omega_B^2 \gg C_1$, C_2 , C_7 , so that the parametric pumping coefficient λ is essentially proportional to C_d . Frequency responses are obtained for $aR/\Delta = 0.2$ and $\Omega/\omega_B = 2 \times 10^{-4}$. The dashed curve is the non-amplified response $(C_d = 0)$, while the red and blue curves correspond to the sense mode frequency responses with $C_d/\omega_B^2 = -0.5 \times 10^4$, -1.1×10^4 respectively; these numbers are chosen such that analytical results of Section 3.3 remain valid, that is, the stated approximations hold. Signal amplification from the intermodal coupling is evident. (For interpretation of the references to color in this figure legend, the reader is referred to the web version of this article.)

equations of motion Eqs. (10a) and (10b) must be used. In this work, however, we restrict our analysis to the case where the response of the sense mode remains in its linear range and its vibration amplitude remains proportional to Ω . In fact, this is the range of practical interest.

3.4. Example

Generally speaking, one can adapt the approach developed here to a variety of gyroscope configurations that exploit circular symmetry. Here we illustrate the applicability of the results by using parameters derived for the polysilicon ring gyroscope reported in [18]. First, we consider the idealized case of a free (no suspension) gyroscope ring. The gyroscope parameters are as follows: the mid-line radius of the ring is $R=550~\mu\text{m}$, the radial thickness is $h=4~\mu\text{m}$, the electrode gap size is $\Delta=1.4~\mu\text{m}$, the estimated quality factor is Q=1200, and the bias voltage is taken to be $V_{DC}=3~\text{V}$ (we intentionally take this value of V_{DC} , as compared to 7 V in [18], to avoid the electrostatic pull-in effect). As a result, the gyroscope dynamic parameters become $\omega_B/2\pi=12.5~\text{kHz},~\Gamma_B/\omega_B=1/2400$ and the electrostatic potential strongly dominates the strength of the dispersive modal coupling, $C_d/\omega_B^2\sim-10^5$, while the other constants defined in Eq. (10b) satisfy C_T , C_1 , $C_2\ll C_d/\omega_B^2$.

Figs. 6a and 6b show the self-induced parametric gain G as a function of the normalized drive frequency ω/ω_B and the normalized vibration amplitude of the drive mode aR/Δ (left panel) and the normalized strength of the stiffness coupling C_a/ω_B^2 (right panel). The solid red curve depicts the instability condition, (a^*, ω^*) in both panels, where the value of the gain approaches infinity, that is, it is the Arnold tongue for the sense mode [49,50]. The meshed region on both panels corresponds to the set of operating conditions where the solution found in Eq. (16) is unstable. In order to describe the gyroscope dynamics in these regions, one must analyze the full form of Eqs. (10a) and (10b), since in this region nonlinear effects that have been ignored will come into play.

As follows from considering the results of Fig. 6a, in order to achieve significant gain G, the drive mode should be operated at frequencies slightly less than ω_B . This can be easily satisfied since the electrostatic forces dominate the nonlinearities of the gyroscopic drive mode and its frequency response exhibits softening behavior. Fig. 6b, on the other hand, illustrates the behavior of the gain G as a function of the operating frequency and the strength of the intermodal dispersive

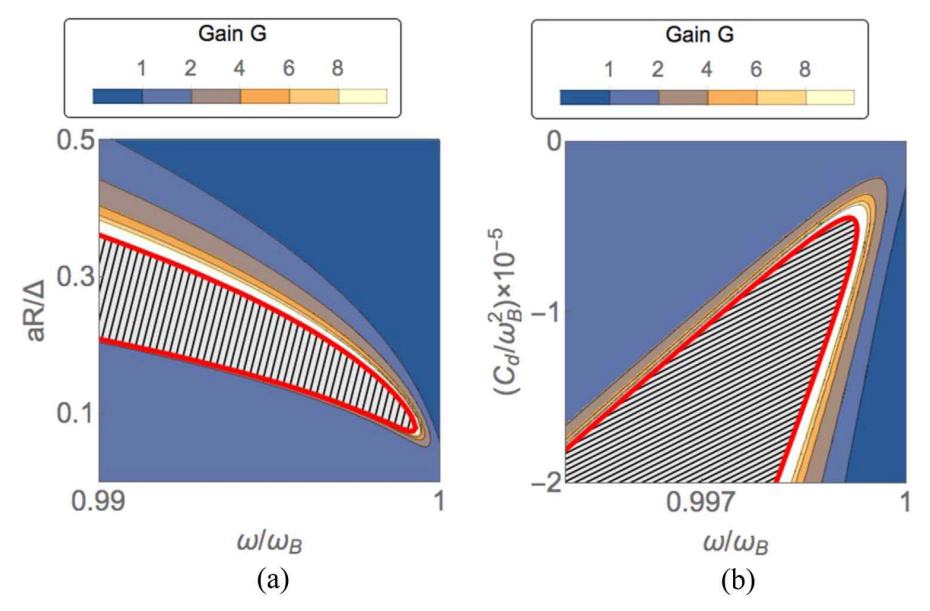


Fig. 6. Increase of the gyroscopic sensitivity of the gyroscope ring (without suspension) due to nonlinear modal coupling as a function of system and drive parameters. The solid red line represents the a^*-a^* curve where the gain G diverges according to the linear model described by Eq. (15); this is the primary Arnold tongue for the sense mode [49]. The meshed region is the set of operating conditions where the solution found in Eq. (16) is unstable: (a) dependence of the strength of the self-induced parametric amplification G on the scaled operation frequency ω/ω_B and the vibration amplitude of the drive mode aR/Δ . The stiffness coupling strength is $C_d/\omega_B^2 = -95 \times 10^3$ and (b) dependence of the strength of the self-induced parametric amplification on the scaled operation frequency ω/ω_B and the nonlinear dispersive coupling strength C_d/ω_B^2 . The drive mode vibration amplitude is chosen to be $aR/\Delta = 0.1$. (For interpretation of the references to color in this figure legend, the reader is referred to the web version of this article.)

coupling. Importantly, the magnitude of the intermodal coupling can be controlled by adjusting the bias voltage V_{DC} applied to the resonator body or attendant electrodes, thus allowing one to tune the amount of self-induced parametric amplification, which increases gyroscope sensitivity S in the vicinity of the instability region. Furthermore, the critical value of the drive mode amplitude, where $G \to \infty$, decreases as $C_d^{-1/2}$. Physically, as expected, this implies that for stronger dispersive intermodal coupling, smaller drive vibration amplitudes are required to achieve the same level of gain.

The results obtained for the case of the unsuspended gyroscope ring can be easily extended to account for supporting springs in the form of semicircles with the mid-line radius $R_s=235~\mu m$ and radial thickness $h=4~\mu m$; see [18] for details. Numerical analysis shows that for the polarization voltage $V_{DC}=7~V$ (the voltage used by Ayazi et al. in their experiments), electrostatic forces still dominate the system nonlinearities, including the dispersive modal coupling strength, $C_d/\omega_B^2\sim -10^4$. As a result, the dependence of the gyroscope sensitivity on the system parameters is qualitatively the same as in the case of the free ring; see Figs. 6a and 6b.

Our analysis of a gyroscope with a suspension shows that the inclusion of the semi-circular suspending springs in the model changes the resonator kinetic and potential energies, where the latter is affected through its elastic component only, since there is no interaction of the springs with the electrodes. Due to the symmetry of the gyroscope elliptical modes, the suspension springs are equivalent to four additional rings of radius R_s , where one pair belongs to the drive mode and the other to the sense mode. In this case, however, when calculating the kinetic energy we also have to account for the motion of the spring mass, which contributes to the effective modal mass. Furthermore, analysis shows that the gyroscope suspension has considerable effect on the individual modal stiffness parameters, affecting both the linear natural frequency and the Duffing nonlinearity. These contributions can be calculated in a straightforward way following the method described in Section 3.1. In particular, the mechanical contributions to the modal natural frequency and the Duffing modal nonlinearity increase by

factors of 5 and 12, respectively. Additionally, the suspension springs also affect the dispersive modal coupling strength; in fact, the mechanical component of κ increases by nearly a factor of two. This contribution to the modal coupling strength is the result of the nonlinear nature of the strain-displacement relationships in Eqs. (5a) to (5c). Similar results for more complicated geometries, such as the disk resonating gyroscope in [22], can be obtained using finite element methods adapted for computing nonlinear coefficients for purely mechanical systems [51,52]. However, finite element methods for computing nonlinear coefficients in systems with electrostatic actuation/sensing are still to be developed.

4. Conclusions

In this work we have analyzed the phenomenon of self-induced parametric amplification of in-plane flexural vibrations of degenerate elliptical modes in ring/disk resonating gyroscopes. The most important feature of this amplification is a gain in sensitivity that is achieved from the naturally occurring dynamics of the system. This is a prime example of where nonlinear behavior provides an opportunity for improved performance of a practical device.

By utilizing the model of a thin spinning ring in the presence of electrostatic actuation/sensing, we have demonstrated that, in addition to the linear Coriolis coupling that is the basis for operation as an angular rate sensor, the drive and sense modes are coupled nonlinearly through elastic, inertial, and electrostatic effects. We have further illustrated that this modal coupling results in parametric pumping of the sense mode by the drive mode, which can lead to a significant improvement in the gyroscope sensitivity with respect to the external angular rate, as was experimentally observed in [22]. We have also examined the effects of the drive conditions on the performance of the sensor, and illustrated these effects for two representative micromechanical ring resonating gyroscopes.

The analytical results presented here can be used for predicting the nonlinear behavior of existing gyroscopes and proposed gyroscope models, and, more importantly, for designing ring/disk resonating gyroscopes with optimized performance and maximized sensitivity using their inherent dynamics.

7301), the US Army Research Office (W911NF-12-1-0235), and the National Science Foundation (1234067). The authors also would like to thank Dave Horsley, Sarah Nitzan, and Tom Kenny for helpful discussions

Acknowledgements

This work was supported by grants from DARPA (FA8650-13-1-

Appendix A. Derivation of nonlinear strain-displacement relationships

Here we derive the nonlinear strain-displacement relationships for $\epsilon_{ij}(u, v)$ presented in Eqs. (5a) to (5c). In order to do so, we consider an infinitesimal segment of the gyroscope body, designated by *KLMN* in with coordinates r and θ and having radial thickness dr and angular length $rd\theta$; see Fig. A.1. This segment can be conveniently defined in terms of the coordinates of its corner points as

$$K = (r, \theta), L = (r + dr, \theta),$$

$$M = (r + dr, \theta + d\theta), N = (r, \theta + d\theta).$$
(A.1)

During operation the body experiences elastic deformations and the segment deforms into $K_1L_1M_1N_1$, which we, in turn, express as

$$K_{1} = \left(r + u(r, \theta), \theta + \frac{v(r, \theta)}{r}\right),$$

$$L_{1} = \left(r + dr + u(r + dr, \theta), \theta + \frac{v(r + dr, \theta)}{r + dr}\right),$$

$$M_{1} = \left(r + dr + u(r + dr, \theta + d\theta), \theta + d\theta + \frac{v(r + dr, \theta + d\theta)}{r + dr}\right),$$

$$N_{1} = \left(r + u(r, \theta + d\theta), \theta + d\theta + \frac{v(r, \theta + d\theta)}{r}\right).$$
(A.2)

From Fig. A.1 it is clear that the strain-displacement relationships $\epsilon_{ij}(u, v)$ are given by

$$\epsilon_{rr} = \frac{K_1 L_1 - KL}{KL}, \ \epsilon_{\theta\theta} = \frac{K_1 N_1 - KN}{KN}, \ \epsilon_{r\theta} = \alpha + \beta. \tag{A.3}$$

Given the coordinate representations of the segment corner points in Eqs. (A.1) and (A.2), we have

KL = dr

$$K_1 L_1 \approx dr \sqrt{\left(1 + \frac{\partial u}{\partial r}\right)^2 + \left(1 + \frac{u}{r}\right)^2 \left(\frac{\partial v}{\partial r}\right)^2},$$
 (A.4a)

 $KN \approx rd\theta$

$$K_1 N_1 \approx r d\theta \sqrt{\left(1 + \frac{u}{r}\right)^2 \left(1 + \frac{\partial v}{r \partial \theta}\right)^2 + \frac{1}{r^2} \left(\frac{\partial u}{\partial \theta}\right)^2},$$
(A.4b)

$$\alpha \approx \frac{r+u}{1+\frac{\partial u}{\partial r}} \frac{\partial}{\partial r} \left(\frac{v}{r}\right), \beta \approx \frac{\frac{\partial u}{\partial \theta}}{(r+u)\left(1+\frac{\partial v}{r\partial \theta}\right)}.$$
(A.4c)

Finally, by using Eqs. (A.4a) to (A.4c) in Eq. (A.3) and expanding the resulting expressions up to the second order in u and v, we obtain the nonlinear strain-displacement relationships given in Eqs. (5a) to (5c).

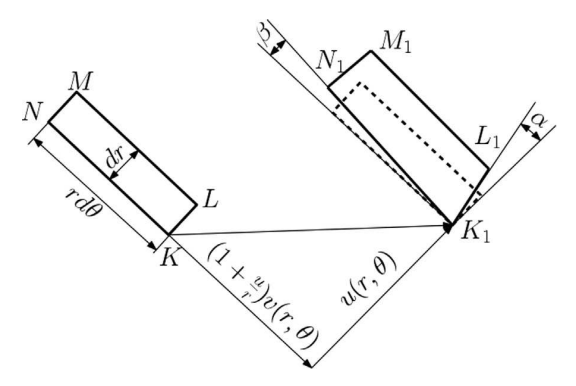


Fig. A.1. Deformation of the gyroscope segment KLMN into $K_1L_1M_1N_1$.

References

- [1] M. Amabili, M.P. Paidoussis, Review of studies on geometrically nonlinear vibrations and dynamics of circular cylindrical shells and panels, with and without fluid-structure interaction, Appl. Mech. Rev. 56 (4) (2003) 349–381. http:// dx.doi.org/10.1115/1.1565084.
- [2] M. Amabili, Nonlinear Vibrations and Stability of Shells and Plates, Cambridge University Press, 2008.
- [3] P.M. Naghdi, The Theory of Shells and Plates, Springer, 1973.
- [4] F. Moussaoui, R. Benamar, Non-linear vibrations of shell-type structures: a review with bibliography, J. Sound Vib. 255 (1) (2002) 161–184. http://dx.doi.org/ 10.1006/isvi.2001.4146.
- [5] A.M. Shkel, Type I and Type II micromachined vibratory gyroscopes, in: Position, Location, and Navigation Symposium, San Diego, 2006, pp. 25–27.
- [6] C. Acar, A. Shkel, MEMS Vibratory Gyroscopes: Structural Approaches to Improve Robustness, Springer Science & Business Media, 2008.
- [7] N. Yazdi, F. Ayazi, K. Najafi, Micromachined inertial sensors, Proc. IEEE 86 (8) (1998) 1640–1659. http://dx.doi.org/10.1109/5.704269.
- [8] J.Y. Cho, J.-K. Woo, J. Yan, R.L. Peterson, K. Najafi, Fused-silica micro birdbath resonator gyroscope (µ-BRG), J. Microelectromech. Syst. 23 (1) (2014) 66–77. http://dx.doi.org/10.1109/JMEMS.2013.2291534.
- [9] I.P. Prikhodko, S.A. Zotov, A.A. Trusov, A.M. Shkel, Microscale glass-blown threedimensional spherical shell resonators, J. Microelectromech. Syst. 20 (3) (2011) 691–701. http://dx.doi.org/10.1109/JMEMS.2011.2127453.
- [10] T. Remtema, L. Lin, Active frequency tuning for micro resonators by localized thermal stressing effects, Sens. Actuators A Phys. 91 (3) (2001) 326–332. http:// dx.doi.org/10.1016/S0924-4247(01)00603-3.
- [11] C.C. Painter, A.M. Shkel, Active structural error suppression in MEMS vibratory rate integrating gyroscopes, IEEE Sens. J. 3 (5) (2003) 595–606. http://dx.doi.org/ 10.1109/JSEN.2003.817165.
- [12] C.H. Ahn, E.J. Ng, V. Hong, Y. Yang, B.J. Lee, I. Flader, T.W. Kenny, Mode-matching of wineglass mode disk resonator gyroscope in (100) single crystal silicon, J. Microelectromech. Syst. 24 (2) (2015) 343–350. http://dx.doi.org/10.1109/ JMEMS.2014.2330590.
- [13] B.J. Gallacher, J. Hedley, J.S. Burdess, A.J. Harris, A. Rickard, D.O. King, Electrostatic correction of structural imperfections present in a microring gyroscope, J. Microelectromech. Syst. 14 (2) (2005) 221–234. http://dx.doi.org/ 10.1109/JMEMS.2004.839325.
- [14] D.J. Kim, R. Closkey, A systematic method for tuning the dynamics of electrostatically actuated vibratory gyros, IEEE Trans. Control Syst. Technol. 14 (1) (2006) 69–81. http://dx.doi.org/10.1109/TCST.2005.860525.
- [15] R. Antonello, R. Oboe, L. Prandi, F. Biganzoli, Automatic mode matching in MEMS vibrating gyroscopes using extremum-seeking control, IEEE Trans. Ind. Electron. 56 (10) (2009) 3880–3891. http://dx.doi.org/10.1109/TIE.2009.2020707.
- [16] S. Wong, C. Fox, S. McWilliam, Thermoelastic damping of the in-plane vibration of thin silicon rings, J. Sound Vib. 293 (1) (2006) 266–285. http://dx.doi.org/ 10.1016/j.jsv.2005.09.037.
- [17] S. Ghaffari, E.J. Ng, C.H. Ahn, Y. Yang, S. Wang, V. Hong, T.W. Kenny, Accurate modeling of quality factor behavior of complex silicon MEMS resonators, J. Microelectromech. Syst. 24 (2) (2015) 276–288. http://dx.doi.org/10.1109/ JMEMS.2014.2374451.
- [18] F. Ayazi, K. Najafi, A HARPSS polysilicon vibrating ring gyroscope, J. Microelectromech. Syst. 10 (2) (2001) 169–179. http://dx.doi.org/10.1109/ 84 925732.
- [19] J.-H. Lee, B.-Y. Choi, K.-h. Park, H.-J. Yoo, Vibrating disk type micro-gyroscope, US Patent 5,783,749, Jul. 21, 1998.
- [20] H. Johari, F. Ayazi, Capacitive bulk acoustic wave silicon disk gyroscopes, in: Electron Devices Meeting, 2006. IEDM'06. International, IEEE, 2006, pp. 1–4. http://dx.doi.org/10.1109/IEDM.2006.346827.
- [21] R.L. Kubena, D.T. Chang, Disc resonator gyroscopes, US Patent 7,581,443, Sep. 1, 2009.
- [22] S.H. Nitzan, V. Zega, M. Li, C.H. Ahn, A. Corigliano, T.W. Kenny, D.A. Horsley, Self-induced parametric amplification arising from nonlinear elastic coupling in a micromechanical resonating disk gyroscope, Sci. Rep. 5 (2015). http://dx.doi.org/10.1038/sren09036
- [23] D. Rugar, P. Grütter, Mechanical parametric amplification and thermomechanical noise squeezing, Phys. Rev. Lett. 67 (6) (1991) 699. http://dx.doi.org/10.1103/ PhysRevLett.67.699.
- [24] J.F. Rhoads, S.W. Shaw, K.L. Turner, R. Baskaran, Tunable microelectromechanical filters that exploit parametric resonance, J. Vib. Acoust. 127 (5) (2005) 423–430. http://dx.doi.org/10.1115/1.2013301.
- [25] J.F. Rhoads, S.W. Shaw, K.L. Turner, J. Moehlis, B.E. DeMartini, W. Zhang, Generalized parametric resonance in electrostatically actuated microelectromechanical oscillators, J. Sound Vib. 296 (4) (2006) 797–829. http://dx.doi.org/ 10.1016/j.jsv.2006.03.009.

- [26] A. Tondl, Autoparametric Resonance in Mechanical Systems, Cambridge University Press. 2000.
- [27] J. Warminski, K. Kecik, Autoparametric vibrations of a nonlinear system with pendulum, Math. Probl. Eng. (2006), http://dx.doi.org/10.1155/MPE/2006/ 80705
- [28] S. Fatimah, M. Ruijgrok, Bifurcations in an autoparametric system in 1: 1 internal resonance with parametric excitation, Int. J. Non-Linear Mech. 37 (2) (2002) 297–308. http://dx.doi.org/10.1016/S0020-7462(00)00115-3.
- 29] A.H. Nayfeh, D.T. Mook, Nonlinear Oscillations, John Wiley & Sons, 2008.
- [30] H. Westra, M. Poot, H. Van der Zant, W. Venstra, Nonlinear modal interactions in clamped-clamped mechanical resonators, Phys. Rev. Lett. 105 (11) (2010) 117205. http://dx.doi.org/10.1103/PhysRevLett.105.117205.
- [31] T. Dunn, J.-S. Wenzler, P. Mohanty, Anharmonic modal coupling in a bulk micromechanical resonator, Appl. Phys. Lett. 97 (12) (2010) 123109. http:// dx.doi.org/10.1063/1.3489423.
- [32] M. Matheny, L. Villanueva, R. Karabalin, J.E. Sader, M. Roukes, Nonlinear mode-coupling in nanomechanical systems, Nano Lett. 13 (4) (2013) 1622–1626. http://dx.doi.org/10.1021/nl400070e.
- [33] Y. Yang, E. Ng, P. Polunin, Y. Chen, S. Strachan, V. Hong, C.H. Ahn, O. Shoshani, S. Shaw, M. Dykman, T. Kenny, Experimental investigation on mode coupling of bulk mode silicon MEMS resonators, in: Micro Electro Mechanical Systems (MEMS), 2015 Proceedings of the 28th IEEE International Conference on, IEEE, 2015, pp. 1008–1011. http://dx.doi.org/10.1109/MEMSYS.2015.7051132.
- [34] D.A. Evensen, Nonlinear flexural vibrations of thin circular rings, J. Appl. Mech. 33 (3) (1966) 553–560. http://dx.doi.org/10.1115/1.3625121.
- [35] A. Maewal, Nonlinear harmonic oscillations of gyroscopic structural systems and the case of a rotating ring, J. Appl. Mech. 48 (3) (1981) 627–633. http://dx.doi.org/ 10.1115/1.3157685.
- [36] S. Natsiavas, Dynamics and stability of non-linear free vibration of thin rotating rings, Int. J. Non-Linear Mech. 29 (1) (1994) 31–48. http://dx.doi.org/10.1016/ 0020-7462(94)90050-7.
- [37] W. Kim, J. Chung, Free non-linear vibration of a rotating thin ring with the in-plane and out-of-plane motions, J. Sound Vib. 258 (1) (2002) 167–178. http://dx.doi.org/ 10.1006/jsvi.2002.5104.
- [38] C. Ahn, S. Nitzan, E. Ng, V. Hong, Y. Yang, T. Kimbrell, D. Horsley, T. Kenny, Encapsulated high frequency (235 kHz), high-Q (100 k) disk resonator gyroscope with electrostatic parametric pump, Appl. Phys. Lett. 105 (24) (2014) 243504. http://dx.doi.org/10.1063/1.4904468.
- [39] W. Soedel, Vibrations of Shells and Plates, CRC Press, 2004.
- [40] C.I. Park, Frequency equation for the in-plane vibration of a clamped circular plate, J. Sound Vib. 313 (1) (2008) 325–333. http://dx.doi.org/10.1016/ j.jsv.2007.11.034.
- [41] W. Weaver Jr, S.P. Timoshenko, D.H. Young, Vibration Problems in Engineering, John Wiley & Sons, 1990.
- [42] S.P. Maganty, W. Bickford, Large amplitude oscillations of thin circular rings, J. Appl. Mech. 54 (2) (1987) 315–322. http://dx.doi.org/10.1115/1.3173014.
- [43] W. Zhang, K.L. Turner, Application of parametric resonance amplification in a single-crystal silicon micro-oscillator based mass sensor, Sens. Actuators A: Phys. 122 (1) (2005) 23–30. http://dx.doi.org/10.1016/j.sna.2004.12.033.
- [44] N.N. Bogolyubov, Y.A. Mitropolskii, Asymptotic methods in the theory of non-linear oscillations, Vol. 10, CRC Press, 1961.
- [45] A.H. Nayfeh, M.I. Younis, E.M. Abdel-Rahman, Dynamic pull-in phenomenon in MEMS resonators, Nonlinear Dyn. 48 (1–2) (2007) 153–163. http://dx.doi.org/ 10.1007/s11071-006-9079-z.
- [46] F.M. Alsaleem, M.I. Younis, L. Ruzziconi, An experimental and theoretical investigation of dynamic pull-in in MEMS resonators actuated electrostatically, J. Microelectromech. Syst. 19 (4) (2010) 794–806. http://dx.doi.org/10.1109/ JMEMS.2010.2047846.
- [47] S.N. Mahmoodi, N. Jalili, S.E. Khadem, An experimental investigation of nonlinear vibration and frequency response analysis of cantilever viscoelastic beams, J. Sound Vib. 311 (3) (2008) 1409–1419. http://dx.doi.org/10.1016/j.jsv.2007.09.027.
- [48] M. Crespo da Silva, C. Glynn, Nonlinear flexural-flexural-torsional dynamics of inextensional beams, J. Struct. Mech. I. Equ. Motion 6 (4) (1978) 437–448. http:// dx.doi.org/10.1080/03601217808907348.
- [49] J. Guckenheimer, P. Holmes, Nonlinear oscillations, dynamical systems, and bifurcations of vector fields, Vol. 42, Springer Science & Business Media, 2013.
- [50] K.L. Turner, S.A. Miller, P.G. Hartwell, N.C. MacDonald, S.H. Strogatz, S.G. Adams, Five parametric resonances in a microelectromechanical system, Nature 396 (6707), 1998, pp. 149–152. http://dx.doi.org/10.1038/24122.
- [51] S. Dou, B.S. Strachan, S.W. Shaw, J.S. Jensen, Structural optimization for nonlinear dynamic response, Philos. Trans. R. Soc. A 373 (2051) (2015) 20140408.
- [52] A. Tripathi, A.K. Bajaj, Computational synthesis for nonlinear dynamics based design of planar resonant structures, J. Vib. Acoust. 135 (5) (2013) 051031. http:// dx.doi.org/10.1115/1.4024845.